Ab Initio Studies on the Stopping Power of Warm Dense Matter with Time-Dependent Orbital-Free Density Functional Theory

Y. H. Ding, A. J. White, S. X. Hu, O. Certik, and L. A. Collins

Ab-initio Studies on the Stopping Power of Warm Dense Matter with Time-Dependent Orbital Free Density Functional Theory

Y. H. Ding[1], A. J. White[2], S. X. Hu[1,*], O. Certik[3], and L. A. Collins[2]

[1]Laboratory for Laser Energetics, University of Rochester, 250 E. River Road, Rochester, NY 14623, USA

*Email: shu@lle.rochester.edu

[2]Theoretical Division, Los Alamos National Laboratory, Los Alamos, NM 87545, USA

[3]Computational and Computer Science Division, Los Alamos National Laboratory, Los Alamos, NM 87545, USA

Electronic transport properties of warm dense matter, such as electrical/thermal conductivities and nonadiabatic stopping power, are of particular interest to geophysics, planetary science, astrophysics, and inertial confinement fusion (ICF). One example is the α-particle stopping power of dense deuterium–tritium (DT) plasmas, which must be precisely known for current small-margin ICF target designs to ignite. We have developed a time-dependent orbital-free density functional theory (TD-OF-DFT) method for *ab initio* investigations of the charged-particle stopping power of warm dense matter. Our current dependent TD-OF-DFT calculations have reproduced the recently well-characterized stopping power experiment in warm dense beryllium. For α-particle stopping in warm and solid-density DT plasmas, the *ab initio* TD-OF-DFT simulations show a lower stopping power up to ~25% in comparison with three stopping-power models often used in the high-energy-density physics community.

PACS numbers: 52.25.Fi, 52.25.Tx, 52.65.-y

Electronic stopping of swift ions by materials has been studied since the beginning of the 20th century [1–3]. The process is relevant to many applications, including biomedical imaging [4], ion therapies [5], radiation protection [6], material damage [7], and many astronomical processes such as stellar and disc accretion [8]. One specific example is the α-particle stopping power of dense deuterium–tritium (DT) plasmas [9–11], where an uncertainty of ~20% in stopping power could lead to a ±50% variation in the energy required for ignition [12]. Accurate stopping power is therefore a key component for hydrodynamic modeling of ICF, astrophysics, and other fusion processes.

A combination of simplified models, analytical limits, and semi-empirical approaches have historically determined the stopping-power of materials [11,13–16]. For low-temperature or high-density systems, first-principles methods based on a quantum mechanical treatment of the electrons provide accurate static, transport, and conductive properties. These methods include finite-temperature density functional theory (DFT)-based quantum molecular dynamics (QMD) [17–22], path-integral Monte Carlo [23–25], and quantum Monte Carlo [26]. In particular, the Kohn–Sham (KS) orbital-based DFT method has been extensively used to calculate transport properties for various materials, including both ionic and electronic transport in the time-independent formalism [18,19,22,27–36]. In addition, the Kohn–Sham time-dependent DFT method has recently been applied to x-ray Thompson scattering (XRTS) [37] and the stopping power of materials well below the Fermi temperatures (T_F) [38].

Strong many-body coupling and quantum electron-degeneracy effects play essential roles in determining material properties in the WDM regime [39-45], which renders the traditional plasma-physics models no longer valid. *Ab initio* approaches which can treat crossover regimes, without system specific corrections, are thus highly desirable. Unfortunately, extending the Kohn–Sham DFT approach beyond T_{F} becomes computationally difficult because of the large number of occupied eigenstates required. For example, recent stopping-power experiments [46,47] performed with warm dense plasmas ($T > T_{\mathrm{F}}$) present particular difficulties. Despite these and other experiments [48–50], as well as theoretical studies [14-16,51–53], a stringent test of stopping-power models with first-principles simulations in the WDM regime remains elusive.

In this Letter, we offer a prescription to extend DFT methods for stopping power to high temperatures and densities through a time-dependent *orbital-free* (OF) formulation. In addition, we introduce a current-dependent (CD) dynamic kinetic energy functional that can initiate dissipation critical to near Bragg peak stopping power. We verify this method by calculating the proton stopping power of warm-dense Be targets recently determined by well-characterized experiments [46]. We then compare our results with predictions from three stopping-power models, Li–Petrasso [11] (LP), Brown–Preston–Singleton [14,15] (BPS), and RPA Dielectric Function [16] (DF), for both the Be experiment and the proposed α-particle stopping in DT.

The orbital-free formalism [54] is based on the original idea of DFT, that is, the total free-energy of a multi-electron system can be written as a functional of electron density $F_{\mathrm{e}}\,[n(\mathbf{r})]$. We define a "collective orbital" $\psi(\mathbf{r})$ as $|\psi(\mathbf{r})|^2 = n(\mathbf{r})$, where $n(\mathbf{r})$ is the total electron density. Note that the introduction of the single "orbital" rather than density

is for numerical convenience. Using the normalization constraint, $\int \left| \psi(\mathbf{r}) \right|^2 d\mathbf{r} = N$, for N

total electrons we can minimize the free-energy functional with respect to $\psi(\mathbf{r})$, through

$\delta \left\{ F_e \left[n(\mathbf{r}) \right] - \mu \int \left| \psi(\mathbf{r}) \right|^2 d\mathbf{r} \right\} \Big/ \delta \psi(\mathbf{r}) = 0$. The Lagrange multiplier, μ, is the chemical

potential of the system. The minimization procedure yields a nonlinear *Schrödinger-like*

equation of the form $H\psi(\mathbf{r}) = \mu\psi(\mathbf{r})$, with the "chemical-potential operator", H, defined

as:

$$H\left[n(\mathbf{r}) \right] = -\frac{1}{2}\nabla^2 + V_{\text{eff}}(\mathbf{r}) = -\frac{1}{2}\nabla^2 + \frac{\delta F_{\text{TF}}}{\delta n(\mathbf{r})}$$

$$+ V_{\text{ei}}(\mathbf{r}) + \int d\mathbf{r}' \frac{n(\mathbf{r}')}{\left| \mathbf{r} - \mathbf{r}' \right|} + \frac{\delta F_{\text{xc}}}{\delta n(\mathbf{r})}$$

(1)

with F_{TF} the Thomas–Fermi (TF) kinetic-energy functional and F_{xc} the exchange-

correlation energy (XC) functional, usually determined in a local density approximation

[55]. The third and fourth terms in Eq. (1) describe potentials from electron–ion and

mean-field electron–electron Coulomb interactions, respectively. The Laplacian operator

arises from the minimization of the von Weizsäcker term [56]. We refer to this

Hamiltonian as TFW.

To extend the OF formalism to time-dependent interactions, we introduce the

velocity field, $\mathbf{u}(\mathbf{r})$, or current, $\mathbf{J}(\mathbf{r}) \equiv n(\mathbf{r})\mathbf{u}(\mathbf{r})$, as an additional variable. The time-

dependent "collective orbital", $\psi(\mathbf{r},t) \equiv \sqrt{n(\mathbf{r},t)}e^{iS(\mathbf{r},t)}$, contains the information from

the scalar velocity field, $\nabla S(\mathbf{r}) = \mathbf{u}(\mathbf{r})$. The "orbital" for all electrons is only a function of

electronic density and velocity, which define the time dependent electronic system

according to the Runge-Gross theorem and the continuity equation. As an ***analog*** to the time-dependent Schrödinger equation, the TD-OF-DFT equation can be written as

$$i\frac{\partial \psi(\mathbf{r},t)}{\partial t} = \left[-\frac{1}{2}\nabla^2 + V_{\text{eff}}(\mathbf{r},t) + V_{\text{dyn}}(\mathbf{r},t) \right]\psi(\mathbf{r},t) \tag{2}$$

with the nonlinear effective potential defined in Eq. (1), given an instantaneous electron density, $V_{\text{eff}}(\mathbf{r},t) = V_{\text{eff}}(\mathbf{r})\big|_{n(\mathbf{r},t)}$. To capture the low-frequency (ω), long-wavelength (q), current response we introduce a CD dynamic kinetic energy potential (functional derivative):

$$V_{\text{dyn}}(\mathbf{r},t) = \frac{\pi^3}{2K_{\text{F}}^2(\mathbf{r},t)}\mathcal{F}^{-1}\left[i\mathbf{q}\cdot\tilde{\mathbf{J}}(\mathbf{q},t)\big/|q|\right] \tag{3}$$

derived from the inverse dynamic Lindhard susceptibility. $\mathcal{F}$ is the Fourier transform operator, and $\tilde{\mathbf{J}}$ is the Fourier-transformed current. $K_{\text{F}}(\mathbf{r,t})$ is a generalized Fermi momentum which depends on the time-dependent density, $K_{\text{F}}(\mathbf{r,t}) = [3\pi^2 n(\mathbf{r},t)]^{1/3}$. For plasmas with a high degeneracy parameter, $\theta \equiv T/T_F = 2k_B T/k_F^2$, a temperature dependence is required in the TF and the CD functionals. We replace the zero-temperature TF functional with the TF-Perrot functional [57] and introduce a scaling function for the CD functional:

$$V_{\text{dyn}}(\mathbf{r},t,T) = \left[1 + a\Theta(\mathbf{r},t,T)^b\right]^{1/b} V_{\text{dyn}}(\mathbf{r},t,T=0). \tag{4}$$

Parameters $a = 2.865$ and $b = 1.8$ are determined from fitting the inverse finite temperature Lindhard susceptibility over a range of temperatures and densities [58]. We define a generalized degeneracy parameter that depends on the time-dependent density

$\Theta(\mathbf{r},t,T) = 2k_B T \big/ K_F^2(\mathbf{r},\mathbf{t})$. This approach yields the dynamic analog to the development of static ($\omega = 0$) kinetic energy functionals [59,60]. If the TF, XC, and CD functionals in Eq. (1) are ignored, then Eq. (2) is equivalent to the Madelung equation [61]. More generally, Eq. (2) is an extended quantum-hydrodynamics formulation [58,62–66].

For the periodic systems considered, we can solve Eqs. (1)–(4) using a split-operator method [67] for both the background plasma and the projectile. We then calculate the stopping power as the average force on the projectile [38]. Note that the TD-OF-DFT method is all-electron and all-ion, treating the electronic structure of the whole system with the same level of theory. No "partial-charge" or "bound *vs* free" electrons need to be defined for the projectile or bulk ions. We use a range of 64 to 1024 atoms in a periodic rectangular box (2–32:1:1) of up to 130-Å length along the long side, depending on the projectile velocity. Box size, grid density, and time step are converged in our calculations. Additionally, for high projectile velocities, $v_\mathrm{p} \square k_F/m_\mathrm{p}$, we calculate the electron–ion force in real space since image effects can become substantial even for the large box sizes.

We first simulate the recent stopping-power measurement in warm dense Be [46]. The experiment was conducted on OMEGA with a 532-μm-long solid Be plug, isochorically heated by x rays produced by a laser-irradiated Ag-coated CH tube. A typical temperature of $k_B T \approx 32$ eV is inferred from XRTS in a similar experimental setup [68]. A D^3He-filled glass capsule is imploded to generate the ~15-MeV protons as the charged-particle source for probing the warm dense Be target. Once the protons passed through the Be target, the spectra of decelerated protons were recorded. At this condition ($\rho = 1.78$ g/cm^3 and $k_B T = 32$ eV), the Be plasma is in its fluid phase [69] with

degeneracy and coupling parameters of $\theta \approx 2$ and $\Gamma \square 0.3$. To start our TD-OF-DFT calculation we randomly take snapshot of the Be plasma as the initial condition, then launch the energetic testing proton to move across it. To illustrate, we show in Fig. 1 the time-dependent electron densities on the x–y plane containing the proton (E_0 = 1 MeV). The high-density "red spots" represent the locations of the background Be ions, while the proton (marked by the arrows) moves toward the +x direction.

We first examine the general effect of our CD functional on stopping power near the Bragg peak. In Fig. 2(a), we compare the energy-dependent stopping powers of Be for the CD ($V_{dyn} \neq 0$) and the TFW ($V_{dyn} = 0$) methods, averaged over multiple initial positions. At velocities near the Bragg peak, the plasma degeneracy plays an important role. We observe that the TFW shows a complete loss of electronic stopping power at low velocities. The CD result shows a linear electronic stopping power at low velocities, which is qualitatively observed in theoretical and experimental stopping-power spectra [11,13,47,70,71]. At velocities significantly higher than the Bragg peak velocity, the TFW and CD results begin to converge. As the proton traverses the plasma, it accumulates *asymmetric* electron density around itself with higher density behind the proton and some small-density perturbation waves excited in front. This asymmetric electron charge distribution provides a "drag" force that slows the proton, this being the dominant mechanism for high-velocity stopping. The CD potential creates an effective "viscosity" that dampens the oscillations. Physically, this dampening is caused by electron-hole excitations [58], not *explicitly* representable in an orbital-free approach, but *implicitly* affected by the CD functional. In the supplemental materials [72], a movie of

the real-time electron dynamics is shown comparing the TFW and CD approaches for a proton energy of 0.1 MeV.

Launching TD-OF-DFT runs with different proton energies ranging from 2 to 15 MeV, we obtain the proton stopping power of the warm dense Be plasma. The converged results are shown in Fig. 2(b). For each energy point, we have statistically averaged over 20 snapshots from different plasma configurations. The error bar in Fig. 2(b) characterizes the variation from the 20 runs. Our results are compared to the three stopping-power models of LP [11], BPS [14,15] as described in Ref. 15, and DF [16] as described by Eqs. (1) and (16) of Ref. 16, all with full electron density. We found that neither screening of the projectile charge nor applying a classical cutoff improved the DF results. For the experimentally accessible energy range, we provide a more-detailed comparison in the inset of Fig. 2(b). The stopping power calculated by TD-OF-DFT is slightly lower than predictions of the LP model (blue solid line) and the BPS model (red dashed line) by ~5% and ~11% respectively, and higher than predicted by DF (orange dash-dotted line) by ~20%. To directly compare with experimental measurements, we take the stopping-power results from TD-OF-DFT calculations and compute the energy spectrum after the protons have traversed the 532-μm Be target. The spectral comparisons between calculations and experiments are made in Fig. 2(c). The proton source from the experiment is centered at ~15 MeV, as shown by the black dashed line in Fig. 2(c). After passing through the Be target, the protons are downshifted to a lower energy peaked near $E \sim 12.2$ MeV. For visual clarity we only plot the TD-OF-DFT, LP, and BPS spectra. The measured downshifted spectrum (purple long dashed line) is in good agreement with the TD-OF-DFT calculation (within ~20 keV), while both LP and

BPS models predict somewhat larger downshifts than experiment. Namely, the proton peaks predicted by LP and BPS models are further downshifted by ~100 keV and ~200 keV, respectively, than both the experiment and the TD-OF-DFT calculation.

As a further example, we consider α-particle stopping in warm-dense DT plasmas. To ultimately obtain experimental verification of stopping-power models, a uniform and well-characterized DT target is needed. The platform for integrated implosion may not be ideal due to its inhomogeneity. On the other hand, we would like to have stopping-power studies relevant to hot-spot and compressed DT-shell conditions in ICF. A possible solution is to scale the warm solid-density targets to have similar coupling and degeneracy parameters to those of ICF ignition targets. To this end, we envision a 50-μm-thick solid DT slab ($\rho = 0.25$ g/cm^3) that can be isochorically heated to $k_B T = 10$ eV by laser-produced soft x rays (similar to the Be case). XRTS techniques [68,73,74] can be used to measure the plasma temperature. At these conditions, we have a degeneracy parameter $\theta \approx 2.4$ and coupling parameter $\Gamma \approx 0.6$, which are close to the compressed DT-shell condition in ICF targets. With a DT-filled exploding-pusher target implosion, the α-particle source can be generated separately for the stopping-power measurements. Bearing such an experimental scenario in mind, we have performed our TD-OF-DFT calculations with α-particle energies ranging from 0.025 to 4 MeV.

The simulation results are shown by Fig. 3(a), in which the LP, BPS, and DF models are also compared with our TD-OF-DFT calculations. The detailed comparisons are shown in the inset of Fig. 3(a), which indicates the stopping power from TD-OF-DFT calculations is smaller overall than LP, BPS, and DF models by ~16%, ~25%, and ~15% respectively. The TD-OF-DFT results predict greater stopping power than all the models

near the Bragg peak. For such moderately coupled and partially degenerate plasmas, many-body effects become more difficult to account for in analytical models. Similar to the Be case, we also plot the spectral comparisons in Fig. 3(b) for the downshifted α particles. The α-particle source (yellow bars) has a central energy of $E_0 = 3.5$ MeV with a thermal width of $\Delta E \approx 200$ keV. The downshifted α-particle spectra predicted by the LP model (blue) and the BPS model (red) peak at $E_{down} \approx 1.6$ MeV and $E_{down} \approx 1.3$ MeV, respectively. In contrast to these model predictions, our TD-OF-DFT calculations (green) give a downshifted peak at $E_{down} \approx 1.8$ MeV. These large differences ($\Delta E_{down} = 200$ to 500 keV) between the stopping-power models and TD-OF-DFT calculations may readily facilitate experimental verifications since they significantly exceed the current experimental energy resolution ($\Delta E \sim 20$ to 50 keV).

In summary, we have presented a time-dependent orbital-free density-functional-theory formulation to investigate charged-particle stopping power of warm-dense plasmas. We developed a current dependent functional critical to describe the near-peak stopping power. Our comparison to recently measured downshifted spectra of energetic protons passing through the warm dense beryllium plasma agrees to within ~20 keV, while the LP and BPS models somewhat overestimated downshift by ~100 keV and ~200 keV, respectively. Moreover, our TD-OF-DFT calculations indicate that the α-particle stopping power of warm dense DT is less than the LP, BPS, and DF models by ~15% to 25% in the ICF-relevant regime. A possible experimental scenario has been identified, that is, to use a solid DT slab ($\rho = 0.25$ g/cm^3) isochorically heated by laser-produced soft x rays to $k_B T = 10$ eV. Such a target can have the similar coupling/degeneracy condition of the compressed DT shell in ICF ignition targets. If verified by well-

characterized experiments, the lower stopping power of warm dense DT predicted by TD-OF-DFT simulations can have significant implications on current low-margin ICF target designs. These results can readily facilitate additional experiments to further validate/advance our knowledge of transport properties of warm dense matter existing in planetary cores, astrophysical objects, and ICF.

This report was prepared as an account of work sponsored by an agency of the U.S. Government. Neither the U.S. Government nor any agency thereof, nor any of their employees, makes any warranty, express or implied, or assumes any legal liability or responsibility for the accuracy, completeness, or usefulness of any information,

apparatus, product, or process disclosed, or represents that its use would not infringe privately owned rights. Reference herein to any specific commercial product, process, or service by trade name, trademark, manufacturer, or otherwise does not necessarily constitute or imply its endorsement, recommendation, or favoring by the U.S. Government or any agency thereof. The views and opinions of authors expressed herein do not necessarily state or reflect those of the U.S. Government or any agency thereof.

References

1. W. H. Bragg and R. Kleeman, Lond. & Edin. Phil. Mag. & J. of Sci., Series 6 **10**, 318 (1905).

2. H. Bethe, Ann. Phys. **5**, 325 (1930).

3. N. Bohr, *The Penetration of Atomic Particles Through Matter*, The Royal Danish Science Society. Mathematical-Physical Communication, Bd. 18, No. 8 (Munksgaard, Copenhagen, Denmark, 1948).

4. R. Rando, A. Bangert, D. Bisello, A. Candelori, P. Giubilato, M. Hirayama, R. Johnson, H. F. W. Sadrozinski, M. Sugizaki, J. Wyss *et al.*, IEEE Trans. Nucl. Sci. **51**, 1067 (2004).

5. W. Donahue, W. D. Newhauser, and J. F. Ziegler, Phys. Med. Biol. **61**, 6570 (2016).

6. H. Tai, *Comparison of Stopping Power and Range Databases for Radiation Transport Study*, NASA Technical Paper (National Aeronautics and Space Administration, Langley Research Center, Hampton, VA, 1997).

7.   G. Fuchs, F. Studer, E. Balanzat, D. Groult, M. Toulemonde, and J. C. Jousset, Europhys. Lett. **3**, 321 (1987).

8.   J. Frank, A. King, and D. Raine, *Accretion Power in Astrophysics*, 3rd ed. (Cambridge University Press, Cambridge, 2002).

9.   S. Skupsky, Phys. Rev. A **16**, 727 (1977).

10.   G. Maynard and C. Deutsch, Phys. Rev. A **26**, 665 (1982).

11.   C. K. Li and R. D. Petrasso, Phys. Rev. Lett. **70**, 3059 (1993); **114**, 199901(E) (2015).

12.   S. Haan, presented at the Charged Particle Transport Code Comparison, Albuquerque, NM, 24–26 October 2016.

13.   N. R. Arista and A. R. Piriz, Phys. Rev. A **35**, 3450 (1987).

14.   L. S. Brown, D. L. Preston, and R. L. Singleton, Jr., Phys. Rep. **410**, 237 (2005).

15.   R. L. Singleton, Jr., Phys. Plasmas **15**, 056302 (2008).

16.   C. F. Clauser, and N. R. Arista, Phys. Rev. E. **97**, 023202 (2018).

17.   J. Clérouin and J.-F. Dufrêche, Phys. Rev. E **64**, 066406 (2001).

18.   L. A. Collins, S. R. Bickham, J. D. Kress, S. Mazevet, T. J. Lenosky, N. J. Troullier, and W. Windl, Phys. Rev. B **63**, 184110 (2001).

19.   M. P. Desjarlais, Phys. Rev. B **68**, 064204 (2003).

20.   V. Recoules, J. Clérouin, G. Zérah, P. M. Anglade, and S. Mazevet, Phys. Rev. Lett. **96**, 055503 (2006).

21.   B. Holst, R. Redmer, and M. P. Desjarlais, Phys. Rev. B **77**, 184201 (2008).

22.   V. Recoules, F. Lambert, A. Decoster, B. Canaud, and J. Clérouin, Phys. Rev. Lett. **102**, 075002 (2009).

23. D. M. Ceperley, Rev. Mod. Phys. **67**, 279 (1995).

24. B. Militzer and D. M. Ceperley, Phys. Rev. Lett. **85**, 1890 (2000).

25. S. X. Hu, B. Militzer, V. N. Goncharov, and S. Skupsky, Phys. Rev. B **84**, 224109 (2011).

26. J. M. McMahon, M. A. Morales, C. Pierleoni, and D. M. Ceperley, Rev. Mod. Phys. **84**, 1607 (2012).

27. M. P. Desjarlais, J. D. Kress, and L. A. Collins, Phys. Rev. E **66**, 025401 (2002).

28. F. Lambert and V. Recoules, Phys. Rev. E **86**, 026405 (2012).

29. S. X. Hu, L. A. Collins, T. R. Boehly, J. D. Kress, V. N. Goncharov, and S. Skupsky, Phys. Rev. E **89**, 043105 (2014).

30. S. X. Hu, L. A. Collins, V. N. Goncharov, J. D. Kress, R. L. McCrory, and S. Skupsky, Phys. Plasmas **23**, 042704 (2016).

31. A. A. Correa, J. Kohanoff, E. Artacho, D. Sánchez-Portal, and A. Caro, Phys. Rev. Lett. **108**, 213201 (2012); **109**, 069901(E) (2012).

32. A. Schleife, Y. Kanai, and A. A. Correa, Phys. Rev. B **91**, 014306 (2015).

33. A. A. Shukri, F. Bruneval, and L. Reining, Phys. Rev. B **93**, 035128 (2016).

34. V. U. Nazarov, J. M. Pitarke, C. S. Kim, and Y. Takada, Phys. Rev. B **71**, 121106(R) (2005).

35. M. Caro, A. A. Correa, E. Artacho, and A. Caro, Sci. Rep. **7**, 2618 (2017).

36. D. C. Yost, Y. Yao, and Y. Kanai, Phys. Rev. B **96**, 115134 (2017).

37. A. D. Baczewski, L. Shulenburger, M. P. Desjarlais, S. B. Hansen, and R. J. Magyar, Phys. Rev. Lett. **116**, 115004 (2016).

38. R. J. Magyar, L. Shulenburger, and A. D. Baczewski, Contrib. Plasma Phys. **56**, 459 (2016).

39. N. C. Santos, W. Benz, and M. Mayor, Science **310**, 251 (2005).

40. G. Fontaine, P. Brassard, and P. Bergeron, Publ. Astron. Soc. Pac. **113**, 409 (2001); G. Fontaine, P. Brassard, and S. Charpinet, EPJ Web of Conferences **43**, 05011 (2013).

41. S. H. Glenzer, B. J. MacGowan, P. Michel, N. B. Meezan, L. J. Suter, S. N. Dixit, J. L. Kline, G. A. Kyrala, D. K. Bradley, D. A. Callahan *et al.*, Science **327**, 1228 (2010).

42. S. X. Hu, B. Militzer, V. N. Goncharov, and S. Skupsky, Phys. Rev. Lett. **104**, 235003 (2010).

43. A. L. Kritcher, T. Döppner, C. Fortmann, T. Ma, O. L. Landen, R. Wallace, and S. H. Glenzer, Phys. Rev. Lett. **107**, 015002 (2011).

44. F. R. Graziani, V. S. Batista, L. X. Benedict, J. I. Castor, H. Chen, S. N. Chen, C. A. Fichtl, J. N. Glosli, P. E. Grabowski, A. T. Graf *et al.*, High Energy Density Phys. **8**, 105 (2012).

45. S. X. Hu, V. N. Goncharov, T. R. Boehly, R. L. McCrory, S. Skupsky, L. A. Collins, J. D. Kress, and B. Militzer, Phys. Plasmas **22**, 056304 (2015).

46. A. B. Zylstra, J. A. Frenje, P. E. Grabowski, C. K. Li, G. W. Collins, P. Fitzsimmons, S. Glenzer, F. Graziani, S. B. Hansen, S. X. Hu *et al.*, Phys. Rev. Lett. **114**, 215002 (2015).

47. J. A. Frenje, P. E. Grabowski, C. K. Li, F. H. Séguin, A. B. Zylstra, M. Gatu Johnson, R. D. Petrasso, V. Yu. Glebov, and T. C. Sangster, Phys. Rev. Lett. **115**, 205001 (2015).

48. D. H. H. Hoffmann, K. Weyrich, H. Wahl, D. Gardés, R. Bimbot, and C. Fleurier, Phys. Rev. A **42**, 2313 (1990); J. Jacoby, D. H. H. Hoffmann, W. Laux, R. W. Müller, H. Wahl, K. Weyrich, E. Boggasch, B. Heimrich, C. Stöckl, H. Wetzler *et al.*, Phys. Rev. Lett. **74**, 1550 (1995); M. Roth, C. Stöckl, W. Süß, O. Iwase, D. O. Gericke, R. Bock, D. H. H. Hoffmann, M. Geissel, and W. Seelig, Europhys. Lett. **50**, 28 (2000).

49. A. C. Hayes, G. Jungman, A. E. Schulz, M. Boswell, M. M. Fowler, G. Grim, A. Klein, R. S. Rundberg, J. B. Wilhelmy, D. Wilson *et al.*, Phys. Plasma **22**, 082703 (2015).

50. W. Cayzac, A. Frank, A. Ortner, V. Bagnoud, M. M. Basko, S. Bedacht, C. Bläser, A. Blažević, S. Busold, O. Deppert *et al.*, Nat. Commun. **8**, 15693 (2017).

51. P. E. Grabowski, M. P. Surh, D. F. Richards, F. R. Graziani, and M. S. Murillo, Phys. Rev. Lett. **111**, 215002 (2013).

52. J. Kim, B. Qiao, C. McGuffey, M. S Wei, P. E Grabowski, and F. N Beg, Phys. Rev. Lett. **115**, 054801 (2015).

53. Z.-G. Fu, Z. Wang, M.-L. Li, D.-F. Li, W. Kang, and P. Zhang, Phys. Rev. E **64**, 063203 (2016).

54. F. Lambert, J. Clérouin, and G. Zérah, Phys. Rev. E **73**, 016403 (2006).

55. J. P. Perdew and A Zunger, Phys. Rev. B **23**, 5048 (1981).

56. C. F. v. Weizsäcker, Z. Phys. **96**, 431 (1935).

57. F. Perrot, Phys. Rev. A **20**, 586 (1979).

58. G. Giuliani and G. Vignale, *Quantum Theory of the Electron Liquid* (Cambridge University Press, Cambridge, England, 2005).

59. L.-W. Wang and M. P. Teter, Phys. Rev. B **45**, 13196 (1992).

60. D. Neuhauser, S. Pistinner, A. Coomar, X. Zhang, and G. Lu, J. Chem. Phys. **134**, 144101 (2011).

61. E. Madelung, Naturwissenschaften **14**, 1004 (1926).

62. I. Tokatly and O. Pankratov, Phys. Rev. B. **60**, 15550 (1999).

63. N. Crouseilles, P. A. Hervieux, and G. Manfredi, Phys. Rev. B **78**, 155412 (2008).

64. C. Ciracì and F. Della Sala, Phys. Rev. B **93**, 205405 (2016).

65. C. Ciracì, Phys. Rev. B **95**, 245434 (2017).

66. V. B. Gildenburg and I. A. Pavlichenko, Phys. Plasma **24**, 084502 (2017).

67. M. D. Feit, J. A. Fleck, and A. Steiger, J. Comput. Phys. **47**, 412 (1982).

68. S. H. Glenzer, O. L. Landen, P. Neumayer, R. W. Lee, K. Widmann, S. W. Pollaine, R. J. Wallace, and G. Gregori, Phys. Rev. Lett. **98**, 065002 (2007).

69. Y. H. Ding and S. X. Hu, Phys. Plasmas **24**, 062702 (2017).

70. J. F. Ziegler, Nucl. Instrum. Methods Phys. Res. B **219–220**, 1027 (2004).

71. J. M. Pruneda, D. Sánchez-Portal, A. Arnau, J. I. Juaristi, and E. Artacho, Phys. Rev. Lett. **99**, 235501 (2007).

72. See Supplemental Material at [URL will be inserted by publisher] for video of real-time difference from initial electronic density, ambient density 32-eV Be plasma stopping of a 0.1-MeV proton. TFW and CD are compared.

73. S. H. Glenzer, G. Gregori, R. W. Lee, F. J. Rogers, S. W. Pollaine, and O. L. Landen, Phys. Rev. Lett. **90**, 175002 (2003).

74. S. P. Regan, K. Falk, G. Gregori, P. B. Radha, S. X. Hu, T. R. Boehly, B. J. B. Crowley, S. H. Glenzer, O. L. Landen, D. O. Gericke *et al.*, Phys. Rev. Lett. **109**, 265003 (2012).

Figure captions

FIG. 1. Snapshots of electron densities in a zoomed window on the x–y plane from TD-OF-DFT simulations (with CD) of a 1-MeV proton traveling through a warm dense Be plasma of $k_B T = 32$ eV and $\rho = 1.78$ g/cm^3.

FIG. 2. (a) A comparison of TD-OF-DFT calculated proton stopping power by a $k_B T = 32$ eV and ambient-density Be plasma, with (CD) and without (TFW) current dependent dynamic potential, from a single MD snapshot and averaged over initial projectile positions; (b) the TD-OF-DFT calculated proton stopping power in high velocities (away from the Bragg peak) in comparison with three stopping-power models of LP [11], BPS [14,15] and DF [16]; and (c) comparisons of the downshifted proton spectra among the experimental measurements [46], predictions of LP and BPS models, and the TD-OF-DFT calculations.

FIG. 3. (a) The α-particle stopping power of warm dense DT plasmas ($\rho = 0.25$ g/cm^3 and $k_B T = 10$ eV) predicted by TD-OF-DFT calculations (green circles) in compared to the LP, BPS and DF models. (b) The calculated downshifted spectra of α particles passing through the 50-μm DT slab at the same warm dense condition from both TD-OF-DFT simulations (green) and the two stopping-power models (red and blue).
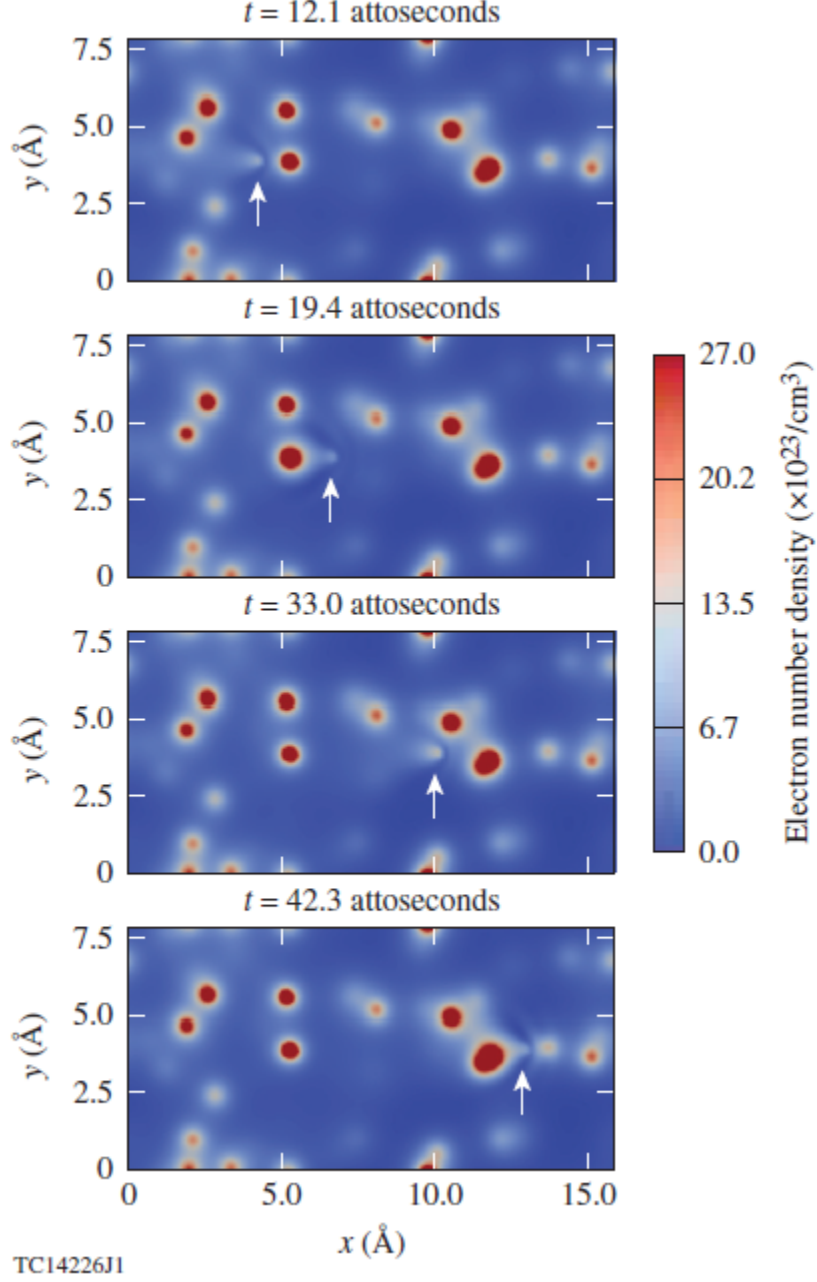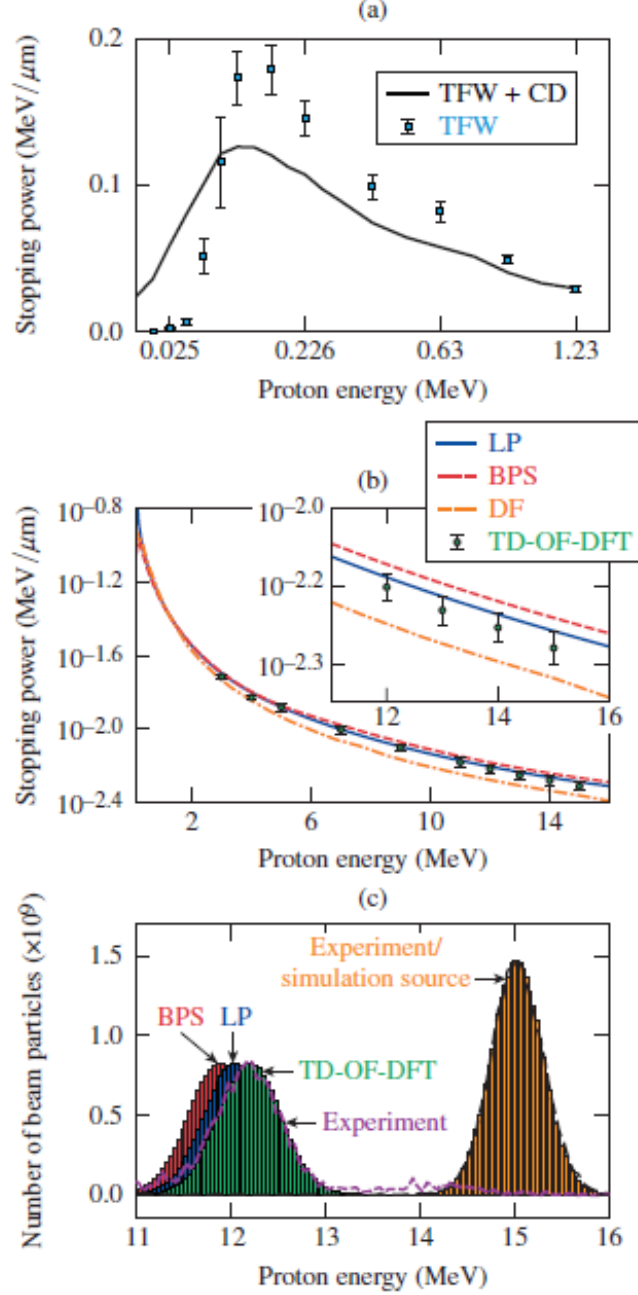
FIG. 1. Snapshots of electron densities in a zoomed window on the x–y plane from TD-OF-DFT simulations (with CD) of a 1-MeV proton traveling through a warm dense Be plasma of $k_B T = 32$ eV and $\rho = 1.78$ g/cm^3.

FIG. 2. (a) A comparison of TD-OF-DFT calculated proton stopping power by a $k_B T = 32$ eV and ambient-density Be plasma, with (CD) and without (TFW) current dependent dynamic potential, from a single MD snapshot and averaged over initial projectile positions; (b) the TD-OF-DFT calculated proton stopping power in high velocities (away from the Bragg peak) in comparison with two stopping-power models of LP [11], BPS [14,15] and DF [16]; and (c) comparisons of the downshifted proton spectra among the experimental measurements [46], predictions of LP and BPS models, and the TD-OF-DFT calculations.
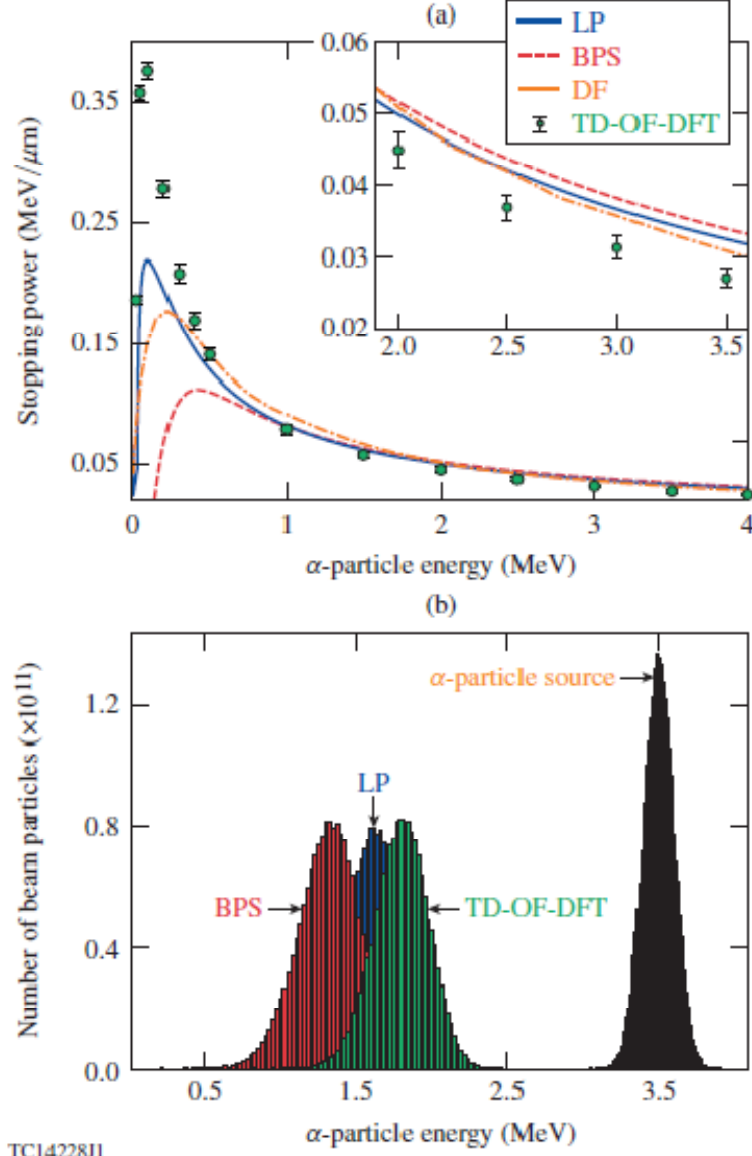
FIG. 3. (a) The α-particle stopping power of warm dense DT plasmas ($\rho = 0.25$ g/cm^3 and $k_B T = 10$ eV) predicted by TD-OF-DFT calculations (green circles) in compared to the LP, BPS and DF models. (b) The calculated downshifted spectra of α particles passing through the 50-μm DT slab at the same warm dense condition from both TD-OF-DFT simulations (green) and the two stopping-power models (red and blue).